

An Acceptor–Donor–Acceptor Structured Small Molecule for Effective NIR Triggered Dual Phototherapy of Cancer

Zheng He, Linlin Zhao, Qiang Zhang, Meijia Chang, Chenxi Li, Hesheng Zhang, Yan Lu,* and Yongsheng Chen*

Dual phototherapy, including photodynamic therapy (PDT) and photothermal therapy (PTT), is regarded as a more effective method for cancer treatment than single PDT or PTT. However, development of single component and near-infrared (NIR) triggered agents for efficient dual phototherapy remains a challenge. Herein, a simple strategy to develop dual-functional small-molecules-based photosensitizers for combined PDT and PTT treatment is proposed through: 1) finely modulating HOMO–LUMO energy levels to regulate the intersystem crossing (ISC) process for effective singlet oxygen ($^1\text{O}_2$) generation for PDT; 2) effectively inhibiting fluorescence via strong intramolecular charge transfer (ICT) to maximize the conversion of photo energy to heat for PTT or ISC process for PDT. An acceptor–donor–acceptor (A–D–A) structured small molecule (CPDT) is designed and synthesized. The biocompatible nanoparticles, FA-CNPs, prepared by encapsulating CPDT directly with a folate functionalized amphipathic copolymer, present strong NIR absorption, robust photostability, cancer cell targeting, high photothermal conversion efficiency as well as efficient $^1\text{O}_2$ generation under single 808 nm laser irradiation. Furthermore, synergistic PDT and PTT effects of FA-CNPs *in vivo* are demonstrated by significant inhibition of tumor growth. The proposed strategy may provide a new approach to reasonably design and develop safe and efficient photosensitizers for dual phototherapy against cancer.

(NIR) light (650–1700 nm), which can minimize light attenuation in tissues, and thus achieving larger penetration depths.^[2–4] The sensitizers for phototherapy are administrated to absorb light energy to produce hyperthermia for PTT or excessive reactive oxygen species (ROS) such as singlet oxygen ($^1\text{O}_2$), hydroxyl radical ($\cdot\text{OH}$), superoxide anion radical ($\text{O}_2^{\cdot-}$), hydrogen peroxide (H_2O_2), etc. for PDT, resulting in the death of cancer cells.^[2,3] It is well known that several PDT photosensitizers (PSs) have approved by the US Food and Drug Administration (FDA) as clinical drugs for some specific indications.^[3] However, the efficacy of PDT is often plagued by hypoxia feature of the tumor microenvironment.^[3,5] While PTT requires high laser powers, which probably leads to other normal tissue damage beyond tumor sites. Therefore, dual phototherapy, that is PDT and PTT combination therapy, is regarded as a safer and more effective method for cancer treatment than single PDT or PTT.

To date, considerable efforts have been devoted to devise multifunctional sensitizing agents for effective single NIR-triggered PDT and PTT combina-

tion therapy.^[6–25] A number of porphyrins and phthalocyanine derivatives-based drugs have been utilized in clinical PDT therapy. Not surprisingly, thus, many efforts are being made to develop new dual phototherapy agents based on these materials.^[6–9] But, their absorption maxima are generally located in visible region, which greatly limits their applications in deep tumor treatment. Besides, deficient photostability and

1. Introduction

Phototherapy, which mainly involves photodynamic therapy (PDT) and photothermal therapy (PTT), has emerged as a minimally invasive, localizing method for efficient cancer therapy.^[1,2] Both PDT and PTT combine usually a nontoxic sensitizing agent with harmless near-infrared

Z. He, Dr. L. L. Zhao, Dr. Q. Zhang, Prof. Y. Lu
School of Materials Science and Engineering
Tianjin Key Laboratory for Photoelectric Materials and Devices
Key Laboratory of Display Materials and Photoelectric Devices
Ministry of Education
Tianjin University of Technology
Tianjin 300384, China
E-mail: luyan@tjut.edu.cn

 The ORCID identification number(s) for the author(s) of this article can be found under <https://doi.org/10.1002/adfm.201910301>.

Dr. M. J. Chang, Prof. C. X. Li, Prof. Y. S. Chen
The Centre of Nanoscale Science and Technology and Key Laboratory of Functional Polymer Materials
State Key Laboratory of Elemento–Organic Chemistry
College of Chemistry
Nankai University
Tianjin 300071, China
E-mail: yschen99@nankai.edu.cn

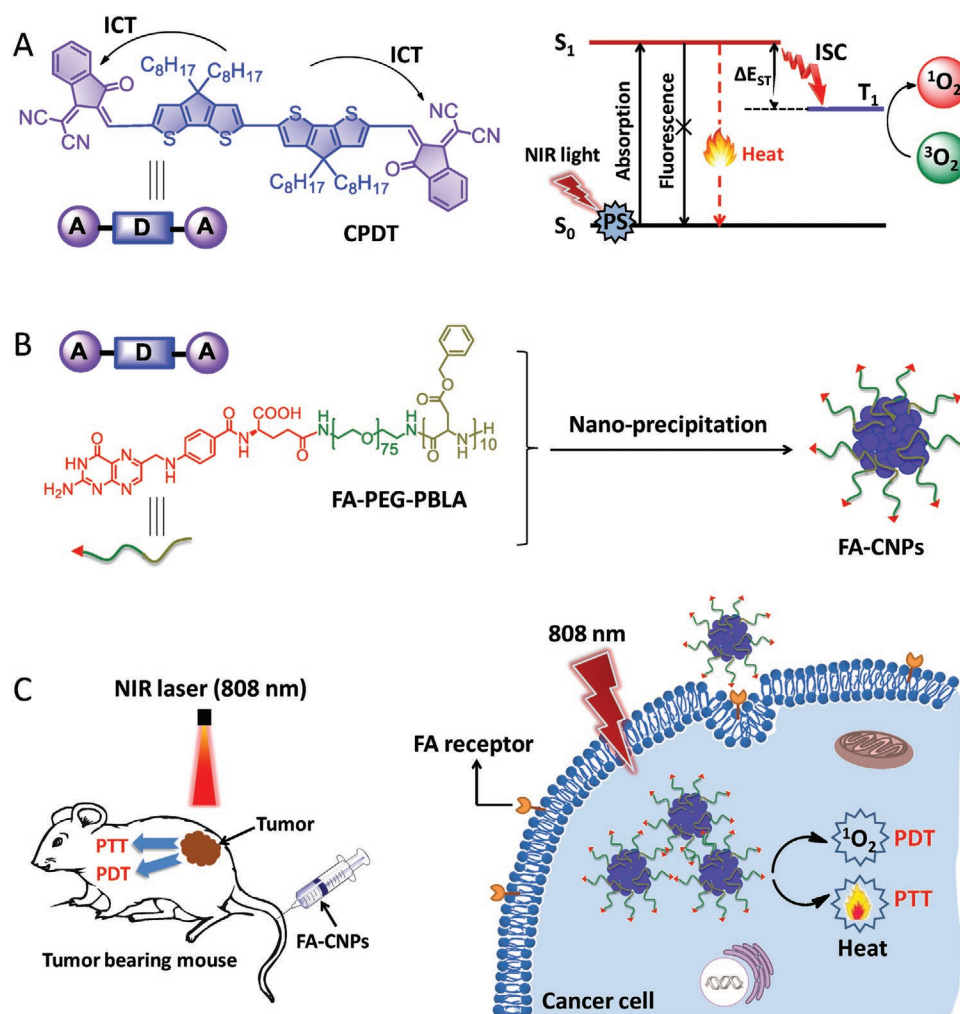
Dr. H. S. Zhang
Tianjin Hemay Biotechnology Co., LTD
Tianjin 300308, China

DOI: 10.1002/adfm.201910301

low photothermal conversion efficiency (PCE) further hinder their clinical translation. Other studies have focused on seeking PDT activity using PTT agents. Thanks to good biocompatibility, easy metabolism, and high structural diversity, many small organic dyes such as cyanines, diketopyrrolopyrrole, boron dipyrromethene, and so on, have been extensively investigated as potential alternative PTT agents.^[10–12] Some of them have exhibited dual PDT and PTT activities with greatly improved efficacy in cancer treatment.^[6–25] Most of them, however, face some unavoidable problems of poor solubility, inferior photostability, short wavelength absorption, low PCE, and tumor targeting ability. So, it is still highly desirable to develop other kinds of sensitizing agents, achieving efficient, and synergistic PDT and PTT therapy under single NIR irradiation.

As shown in Scheme 1A, in order to produce efficiently singlet oxygen ($^1\text{O}_2$) for PDT and heat for PTT, an ideal photosensitizer (PS) should possess the following merits from the perspective of energy conversion: 1) absorbing NIR

light effectively; 2) displaying low fluorescence quantum yield; 3) suitable HOMO–LUMO distribution for sufficient intersystem crossing (ISC) to translate ground-state oxygen ($^3\text{O}_2$) to singlet oxygen ($^1\text{O}_2$).^[26,27] Previous studies have demonstrated that the lower energy gap (ΔE_{ST}) between the lowest excited singlet state (S_1) state and the lowest triplet state (T_1) state, the higher efficiency of ISC.^[28,29] ΔE_{ST} can be finely modulated by manipulating HOMO and LUMO energy levels.^[29] Recently, remarkable progress has been made in the applications of near-infrared photoactivatable semiconducting materials for cancer therapy.^[30–32] In our efforts to develop nonfullerene organic semiconducting materials with an acceptor–donor–acceptor (A–D–A) structure for high-performance organic solar cells,^[33–36] we found that this kind of A–D–A type molecules could fulfill the critical requirements for synergistic PDT and PTT. Benefiting from the strong intramolecular charge transfer (ICT), the A–D–A architecture usually exhibits both broad absorption that can extend to NIR region and effectively suppressed fluorescence. Their HOMO



Scheme 1. Design A–D–A structured molecules for PDT and PTT combination treatment. A) Chemical structure of CPDT and working principle of an ideal photosensitizer for single NIR laser triggered dual phototherapy using a modified Jablonski diagram. B) Schematic illustration of FA-CNPs preparation. C) Schematic illustration of single NIR laser triggered dual phototherapy of tumor based on FA-CNPs.

and LUMO energy levels can be facilely tuned through delicate molecule design.^[33–36] In addition, most recently, A–D–A structured molecule (ITIC)-based nanoparticles have been proven to have PTT effect with high PCE in vitro ($\approx 41.6\%$) under 660 nm laser irradiation.^[37] With this, we believe that it is possible to realize both effective $^1\text{O}_2$ generation for PDT and high PCE for PTT through elaborate design of A–D–A molecules.

On basis of our previous studies about A–D–A type molecules,^[33–36] a new organic semiconducting material (CPDT) was designed and synthesized as a proof-of-concept example considering that its unique optical properties perfectly meet the key requirements of dual-functional sensitizing agents for synergistic PDT and PTT (Scheme 1). To ensure complete fluorescence quenching, good biocompatibility, and effective tumor accumulation, CPDT was directly encapsulated into a folate functionalized amphiphilic copolymer (FA-PEG-PBLA) through nanoprecipitation method, yielding nanoparticles FA-CNPs (Scheme 1B). In this nanoplatform, the folate functionalized FA-PEG-PBLA endows the resulting FA-CNPs with active targeting ability toward cancer cells.^[38,39] FA-CNPs displayed robust photostability, enhanced tumor accumulation ability, high PCE (36.5%), and capacity of $^1\text{O}_2$ generation with the quantum yield of about 18.6% using indocyanine green (ICG) as a standard under 808 nm laser irradiation. The results in vivo demonstrated that FA-CNPs possessed excellent anti-cancer efficacy without distinct damage to the normal tissue (Scheme 1C).

2. Results and Discussion

2.1. Molecular Design and DFT Calculation of ΔE_{ST}

The alkyl-chain-grafted 2,2'-bi(cyclopenta[1,2-*b*:5,4-*b'*]dithiophene) segment as an electron donor and two electron-withdrawing end units 2-(3-oxo-2,3-dihydroinden-1-ylidene)malononitrile (INCN) as electron acceptors were employed to synthesize CPDT. CPDT in CHCl_3 shows a clear absorption peak centered at around 750 nm with a high molar extinction coefficient ($\epsilon = 2.4 \times 10^4 \text{ M}^{-1} \text{ cm}^{-1}$) (Figure 1A). By contrast, its thin film exhibits strong and broad absorption in 500–900 nm regions, implying the potential of CPDT as sensitizer for NIR-triggered phototherapy. Owing to efficient ICT from donor units to acceptor units in the excited state, CPDT in CHCl_3 displays a weak red fluorescence with a low fluorescence quantum yield ($\Phi = 1.7\%$) using rhodamine B as a reference ($\Phi = 0.73$ in ethanol) (Figure 1B). This is favored for dual phototherapy since the absorbed photo energy should have higher portion to generate more heat for PTT and $^1\text{O}_2$ for PDT. The energies of the HOMO, LUMO, and ΔE_{ST} of CPDT are -5.41 , -3.50 , and 0.96 eV, respectively, obtained from DFT calculations (Figure 1C,D). Its narrow bandgap ($E_g = 1.91$ eV) is beneficial for NIR light-absorbing capability.

2.2. FA-CNPs Nanoparticles Formation

To improve biocompatibility and water-solubility of CPDT to realize biological applications, hydrophobic CPDT was directly

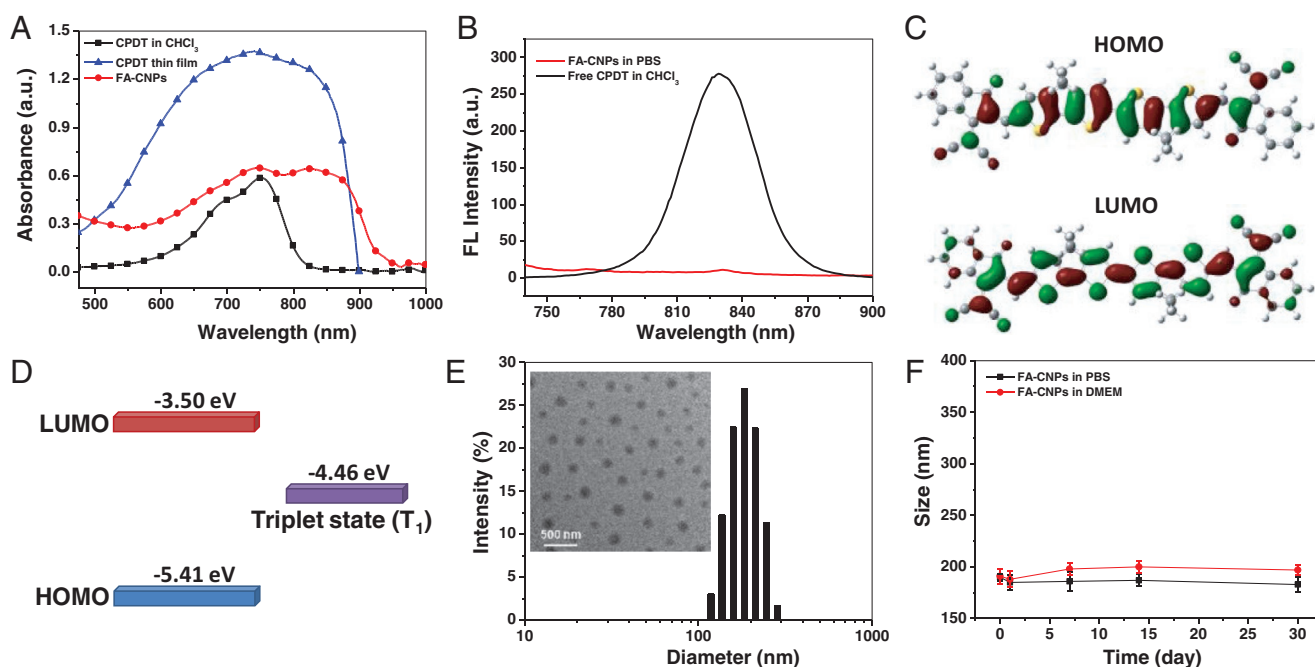


Figure 1. A) UV–vis absorption spectra of CPDT in CHCl_3 ($30 \mu\text{g mL}^{-1}$), CPDT thin film (spin-cast from chloroform solution), and FA-CNPs dispersed in PBS (0.01 M , pH 7.4) ([FA-CNPs] = $180 \mu\text{g mL}^{-1}$, $30 \mu\text{g mL}^{-1}$ based on CPDT). B) Fluorescence spectra of CPDT in CHCl_3 ($30 \mu\text{g mL}^{-1}$) and FA-CNPs dispersed in PBS (0.01 M , pH 7.4) ([FA-CNPs] = $180 \mu\text{g mL}^{-1}$). C, D) Calculated HOMO, LUMO, and triplet state (T_1) energy levels of CPDT using the DFT B3LYP/6-31G(d) method, $E_g = E_{\text{LUMO}} - E_{\text{HOMO}}$. E) DLS data and TEM image (inset) of FA-CNPs nanoparticles. F) Changes of hydrodynamic diameters of FA-CNPs in PBS and Dulbecco’s modified Eagle’s medium (DMEM) with time, [FA-CNPs] = $300 \mu\text{g mL}^{-1}$.

encapsulated into a folate functionalized amphiphilic block copolymer (FA-PEG-PBLA) through a nanoprecipitation process to afford composite nanoparticles FA-CNPs with active targeting ability to cancer cells (Scheme 1B).^[40] The representative transmission electron microscopy (TEM) (inset, Figure 1E) reveals that the as-prepared FA-CNPs have uniform spherical morphology with about 134 ± 9.7 nm in diameter. They can be dispersed well in phosphate buffered saline (PBS) with a hydrodynamic diameter of ≈ 190 nm determined by dynamic light scattering (DLS) (Figure 1E), indicating possibly additional passive targeting ability to tumor by permeation and retention (EPR) effect. Moreover, the size of FA-CNPs in PBS and Dulbecco's modified Eagle's medium (DMEM) (which is the most widely used media for cell and tissue culture) remains almost the same within 30 days, suggesting excellent stability of FA-CNPs nanoparticles (Figure 1F). FA-CNPs in PBS display broad and strong absorption over 750–870 nm, which enables deep penetration into tissue and have potential to achieve effective phototherapy for deep tumor (Figure 1A). Owing to synergic ICT and aggregation-induced quenching, FA-CNPs exhibits negligible fluorescence with a very low fluorescence quantum yield ($\Phi = 0.002\%$) using rhodamine B as a reference ($\Phi = 0.73$ in ethanol), which will greatly benefit the adsorbed photons to dissipate energy in other ways such as heat or ISC process.

2.3. PDT and PTT Effects of FA-CNPs

PTT activity of FA-CNPs was first assessed. As expected, the temperature of FA-CNPs in PBS was effectively and quickly

elevated in concentration-dependent manner under 808 nm laser irradiation at 0.7 W cm^{-2} (Figure 2A). Infrared (IR) thermal images at given irradiation time were also provided in Figure 2B. As shown in Figure 2A,B, when the concentration of FA-CNPs increased to $250 \mu\text{g mL}^{-1}$, the temperature of solution rose rapidly to $72.2 \text{ }^\circ\text{C}$ ($\Delta T = 49.2 \text{ }^\circ\text{C}$) under 808 nm laser irradiation at 0.7 W cm^{-2} for 12 min. It was noted that FA-CNPs as low as $90 \mu\text{g mL}^{-1}$ ($15 \mu\text{g mL}^{-1}$ based on CPDT) also exhibited effective hyperthermia ($47.9 \text{ }^\circ\text{C}$) under the same conditions, which is sufficient to induce apoptosis or necrosis of cancer cells.^[41–43] By contrast, only slight temperature increase by $\approx 0.4 \text{ }^\circ\text{C}$ was observed for the control PBS, indicating excellent PTT capacity of FA-CNPs. Further, influence of laser power density on the temperature changes of FA-CNPs in PBS was estimated (Figure 2C,D). From Figure 2C,D, it was clearly seen that the temperature of FA-CNPs solutions elevated quickly with increasing the power density of laser, suggesting that the temperature changes are linearly correlated with the power density of laser.

The PCE of FA-CNPs was measured to be about 36.5% based on a cycle of heat-cooling according to the reported method (Figure S5 of the Supporting Information for the details).^[44] PCE of FA-CNPs is ≈ 12 -fold higher than that of ICG ($\approx 3.1\%$)^[13] (ICG is an FDA-approved NIR contrast agent and is comparable to previously reported PTT agents such as cyanine dyes ($\approx 26.6\%$) and gold nanorods ($\approx 21.0\%$)).^[45–47]

Subsequently, the ability of $^1\text{O}_2$ generation of FA-CNPs under 808 nm laser irradiation was checked by using 1,3-diphenylisobenzofuran (DPBF) as a probe, since absorption of DPBF

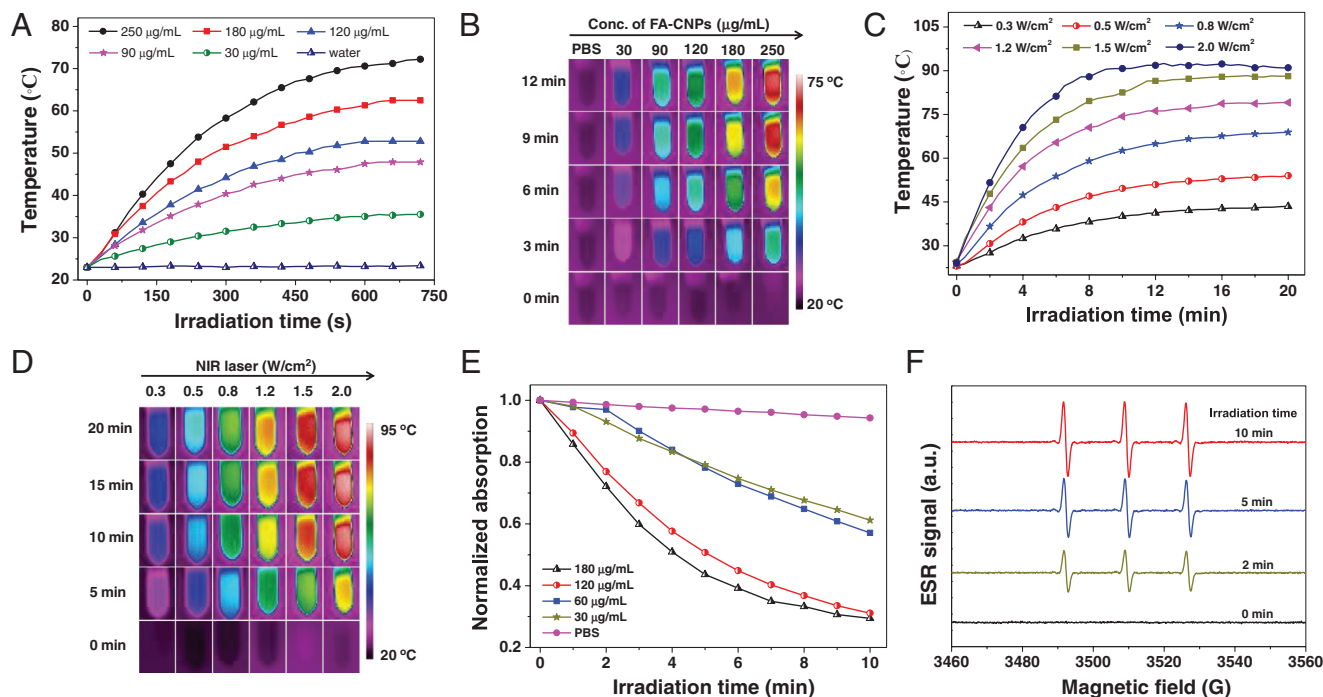


Figure 2. A) Photothermal conversion behavior and B) IR thermal images of FA-CNPs in PBS (0.01 M, pH 7.4) at different concentrations (0– $250 \mu\text{g mL}^{-1}$) under 808 nm irradiation at 0.7 W cm^{-2} . C) Photothermal conversion behavior and D) IR thermal images of FA-CNPs in PBS (0.01 M, pH 7.4) ([FA-CNPs] = $180 \mu\text{g mL}^{-1}$) at different laser power (0.3 – 2.0 W cm^{-2}) under 808 nm irradiation. E) Changes of absorbance at 417 nm of DPBF in presence of different concentrations of FA-CNPs (0 – $180 \mu\text{g mL}^{-1}$) under 808 nm laser irradiation at 0.7 W cm^{-2} with time. F) ESR spectra of FA-CNPs in PBS (0.01 M, pH 7.4) ($180 \mu\text{g mL}^{-1}$) using TEMP as spin-trapping adduct under 808 nm irradiation at 0.7 W cm^{-2} for different time.

will be quickly weakened upon irreversible reaction with $^1\text{O}_2$.^[48] The absorbance of DPBF at 417 nm in presence of FA-CNPs reduced sharply with the increase of FA-CNPs concentrations from 0 to $180 \mu\text{g mL}^{-1}$ (Figure 2E; Figure S6, Supporting Information). The absorption intensity decreased about 69% within 10 min at $[\text{FA-CNPs}] = 120 \mu\text{g mL}^{-1}$ under 808 nm laser irradiation at 0.7 W cm^{-2} , suggesting that $^1\text{O}_2$ could be efficiently generated in this case. The $^1\text{O}_2$ quantum yield (Φ) of FA-CNPs was also determined to be about 18.6% using DPBF and ICG as probe and reference, respectively (Figure S7, Supporting Information).^[47] Moreover, electron spin resonance (ESR) technique was utilized to verify $^1\text{O}_2$ generation using 2,2,6,6-tetramethylpiperidine (TEMP) as a spin-trapping agent. As shown in Figure 2F, after 808 nm laser irradiation for 2 min, the characteristic 1:1:1 multiplicity from TEMP-1-oxyl was observed in the ESR spectra, demonstrating the presence of $^1\text{O}_2$, which was captured by TEMP.^[47] With the increase of irradiation time, the ESR signal enhanced gradually, indicating more $^1\text{O}_2$ generation.

To further confirm that the PTT and PDT activity of FA-CNPs comes from the effective component CPDT, photothermal conversion behavior and $^1\text{O}_2$ generation of free CPDT in THF were also tested as shown in Figure S8 of the Supporting Information. The solution temperature rapidly increases to about $60 \text{ }^\circ\text{C}$ ($\Delta T = 37 \text{ }^\circ\text{C}$) under 808 nm laser irradiation at 0.7 W cm^{-2} for 4 min (Figure S8A, Supporting Information). In addition, quick and effective $^1\text{O}_2$ generation could be observed in the case of free CPDT under irradiation (Figure S8B, Supporting Information). All studies above on photothermal and photodynamic properties of FA-CNPs suggested that FA-CNPs can act as a

promising candidate for PTT and PDT combination therapy under a single NIR 808 nm laser irradiation.

2.4. Photostability of FA-CNPs

The stability against photobleaching was first assessed by continuous irradiation of FA-CNPs in PBS ($180 \mu\text{g mL}^{-1}$, $30 \mu\text{g mL}^{-1}$ based on CPDT) for 30 min using 808 nm laser at 0.7 W cm^{-2} . As shown in Figure 3A, slight decrease in absorption intensity of FA-CNPs solution was observed, accompanied by no obvious solution color change. While the controlled ICG in PBS ($30 \mu\text{g mL}^{-1}$) exhibited significant changes in both UV-absorption spectra and solution color even after shorter irradiation time (15 min). These results demonstrated that FA-CNPs have much more stability against photobleaching than ICG.

Furthermore, its ability to maintain the photothermal effect was checked (Figure 3B,C). In this study, FA-CNPs in PBS ($180 \mu\text{g mL}^{-1}$) suffered from five successive irradiation-cooling cycles. From Figure 3B,C, it can be obviously seen that the highest temperatures were above $60 \text{ }^\circ\text{C}$ for all 5 cycles under 808 nm irradiation at 0.7 W cm^{-2} for 5 min, and their difference is only less than 4%. These results verify that FA-CNPs can remain excellent PTT activity for at least five times. Besides, influence of repeated irradiations with 808 nm laser on $^1\text{O}_2$ generation capability of FA-CNPs was evaluated using DPBF as a probe. In this study, four samples of FA-CNPs in PBS with a concentration of $180 \mu\text{g mL}^{-1}$ were first irradiated by 808 nm laser at 0.7 W cm^{-2} for different time such as 0, 5, 10, 15 min.

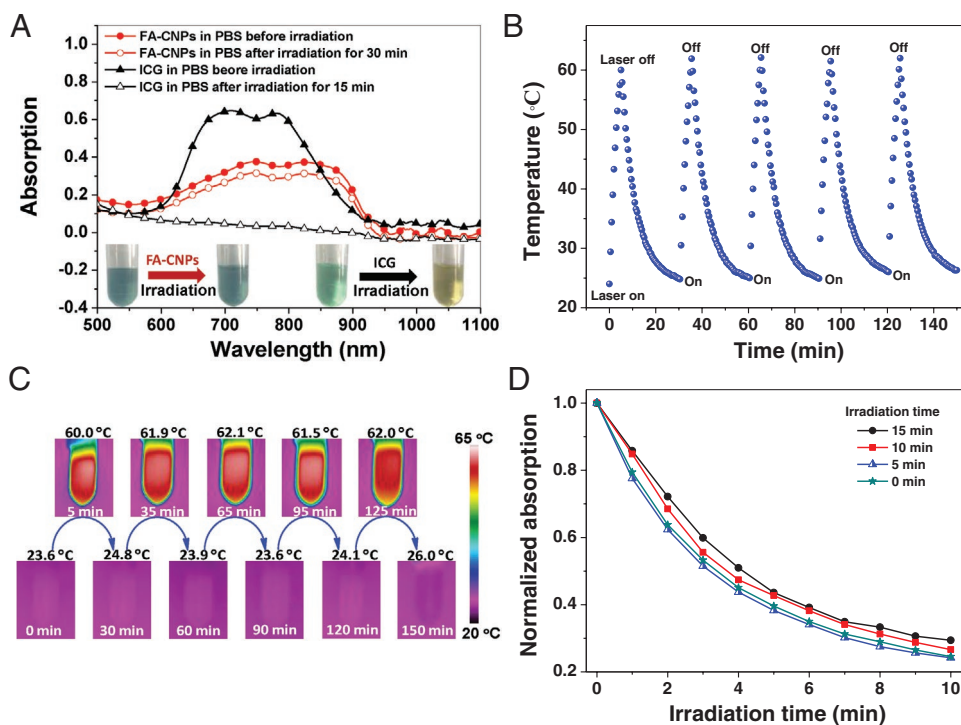


Figure 3. A) UV-vis absorption spectra and photographs of FA-CNPs in PBS and ICG in PBS ($[\text{FA-CNPs}] = 180 \mu\text{g mL}^{-1}$, $30 \mu\text{g mL}^{-1}$ based on CPDT; $[\text{ICG}] = 30 \mu\text{g mL}^{-1}$) before and after continuous irradiation with 808 nm laser at 0.7 W cm^{-2} for 30 and 15 min, respectively. B) Temperature elevation and C) IR thermal images of FA-CNPs in PBS ($180 \mu\text{g mL}^{-1}$) under 5 irradiation/cooling cycles (808 nm laser, 0.7 W cm^{-2} , 5 min). D) Changes of absorption intensity at 417 nm of DPBF in presence of $180 \mu\text{g mL}^{-1}$ of FA-CNPs with reirradiation time (808 nm laser, 0.7 W cm^{-2}).

After this, DPBF was added to the above four samples in the dark. These mixed samples were subsequently re-exposed to 808 nm laser at 0.7 W cm^{-2} for 10 min. During irradiation, UV-vis absorption spectra of probe molecule DPBF were recorded at an interval of 1 min (Figure S9, Supporting Information). The changes of absorbance of DPBF at 417 nm with irradiation time were plotted in Figure 3D. From Figure 3D, it can be clearly seen that the absorption intensity of four samples decreased gradually and the variation trend of absorbance was almost the same. These results suggested that FA-CNPs can still steadily and continuously generate $^1\text{O}_2$ under repeated irradiation.

2.5. Dark Toxicity and Phototoxicity of FA-CNPs

In order to inspect dark toxicity and phototoxicity of FA-CNPs, the internalization behavior of FA-CNPs by tumor cells was first studied. As shown in Figure 4A, cellular uptake of FA-CNPs is linearly dependent on incubation time and the longer incubation time, the higher cellular uptake. After 48 h incubation,

FA-CNPs presented a remarkable cellular uptake. In comparison, CPDT itself only showed insignificant cell internalization probably due to its poor water-solubility. Clearly, FA-CNPs can be preferably internalized by tumor cells. Subsequently, dark toxicity of FA-CNPs was examined with a standard MTT assay. As shown in Figure 4B, viability of HeLa cells was well maintained after incubation with FA-CNPs with different concentrations from 0 to $250 \mu\text{g mL}^{-1}$. More than 85% of cell viability was observed even at FA-CNPs concentration as high as $250 \mu\text{g mL}^{-1}$. These results convincingly revealed the outstanding biocompatibility of FA-CNPs, which is favored for various biomedical applications.

In vitro phototoxicity of FA-CNPs against HeLa cells was then assessed. From Figure 4C, after 808 nm laser irradiation at 0.7 W cm^{-2} for 5 min, more cell apoptosis was found with the increase of FA-CNPs concentrations. More importantly, in the presence of L-ascorbic acid (Vc), FA-CNPs showed slight reduced phototoxicity against HeLa cells because the produced $^1\text{O}_2$ can be scavenged by Vc. By contrast, the coating polymer FA-PEG-PBLA with different concentrations only showed

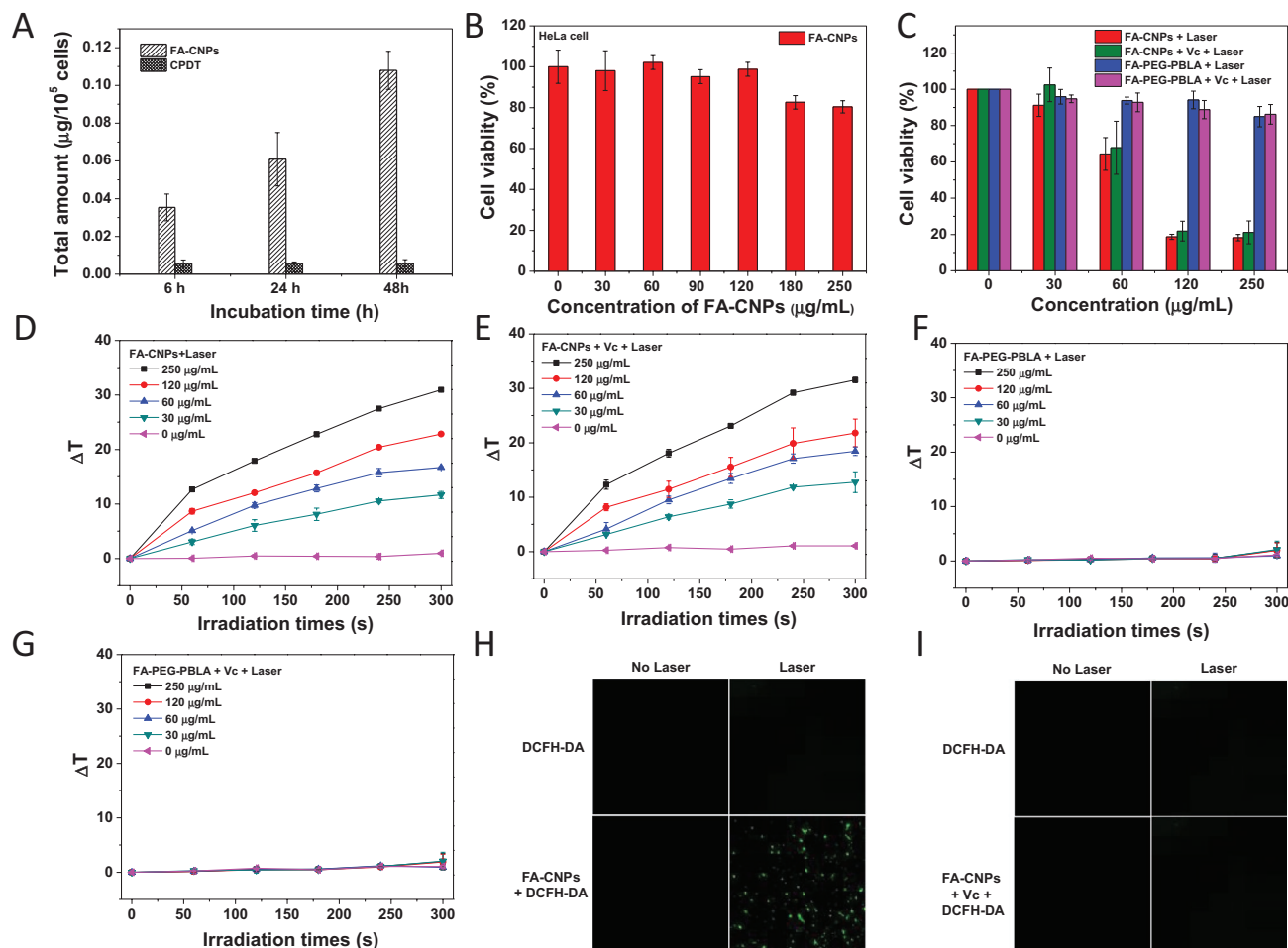


Figure 4. A) Internalized amount of FA-CNPs and CPDT in HeLa cells after 6, 24, and 48 h incubation, respectively. B) Effect of FA-CNPs concentrations on cell viability. C) In vitro phototoxicity against HeLa cells under 808 nm irradiation at 0.7 W cm^{-2} for 5 min. [FA-CNPs] = [FA-PEG-PBLA] = 0– $250 \mu\text{g mL}^{-1}$, [Vc] = $0.1 \times 10^{-3} \text{ M}$. D–G) PTT effect at the cellular level under the same conditions as in (C). H, I) Intracellular $^1\text{O}_2$ monitor of HeLa cells treated with different conditions.

negligible phototoxicity both in the absence or the presence of Vc. All observations from MTT assays distinctly demonstrated that FA-CNPs have both low dark toxicity and high phototoxicity, and could serve as a promising nanoagent for dual phototherapy of cancer.

Furthermore, the PTT and PDT activities of FA-CNPs in HeLa cells were also verified as shown in Figure 4D–I. Significant temperature elevations in concentration-dependent manner were observed for FA-CNPs-contained groups in the absence or the presence of Vc (Figure 4D,E), while there was no clear temperature change under all tested conditions for the control groups (Figure 4F,G). These results indicated there was the PTT activity of FA-CNPs in living cells. In addition, the intracellular $^1\text{O}_2$ generation was evaluated by taking advantage of 2',7'-dichlorofluorescein diacetate (DCFH-DA) as an indicator. Nonfluorescent DCFH-DA can be rapidly converted to green fluorescent product (2',7'-dichlorofluorescein, DCF) in the presence of $^1\text{O}_2$.^[20] As displayed in Figure 4H, HeLa cells incubated with FA-CNPs and DCFHDA exhibited bright green fluorescence upon 808 nm laser irradiation. But no obvious fluorescence was observed in nonirradiated controlled experiment and the case of addition of Vc in above system (Figure 4I). These results indicated that $^1\text{O}_2$ can be efficiently generated in live cells. Therefore, high phototoxicity of FA-CNPs against HeLa cells should be attributed to synergetic PTT and PDT effect in living cells.

2.6. In Vivo Biodistribution and Photothermal Properties

The accumulation of photosensitizers in malignant tissues would greatly enhance the therapeutic efficiency and reduce damage to normal tissues.^[49] Since folic acid, which is a universal targeting group for folate receptors overexpressed on the surface of tumor cells, has been introduced to construct FA-CNPs, its efficient distribution in tumor tissues was expected. We intravenously injected FA-CNPs in PBS ($180 \mu\text{g mL}^{-1}$) into the SK-OV-3 tumors-bearing mice at the dose of 4 mg kg^{-1} , and the bio distributions of efficient component CPDT were measured at 6, 12, 24, and 48 h postinjection by removal of main organs followed by subsequent extraction of CPDT from these tissues using chloroform. Extracted CPDT was then quantified by UV-vis analysis.^[47] As shown in Figure 5A, FA-CNPs exhibited gradually increased accumulation in the tumors site within 6–24 h postinjection and obvious reduced accumulation at 48 h postinjection probably due to the metabolic effect of mice. Relatively high accumulated concentration at lung tissue was also observed, which should be probably attributed to the filtration effect of the lung capillary bed.^[50,51] In addition, it was noted that FA unconjugated controlled sample (CH_3 -CNPs) exhibited obviously lower accumulate concentration in tumor at the same postinjection time than that in the case of FA-CNPs (Figure S10, Supporting Information), indicating that FA groups endows FA-CNPs with active targeting ability to cancer cells as demonstrated by other related research.^[52]

To verify the ability of FA-CNPs to generate hyperthermia in vivo, FA-CNPs in PBS ($180 \mu\text{g mL}^{-1}$) were injected into the SK-OV-3 tumor-bearing mice through the tail vein at

different doses ($0\text{--}12 \text{ mg kg}^{-1}$). After 24 h postinjection, these mice were exposed to 808 nm laser irradiation at 1.0 W cm^{-2} for 5 min. Changes of tumor surface temperature were monitored by infrared thermograph during irradiation. As shown in Figure 5B, the temperature elevation is directly proportional to the doses of FA-CNPs. The dose as low as 4 mg can still trigger the tumor surface temperature rise to $50.5 \text{ }^\circ\text{C}$ under 808 nm laser irradiation for 5 min, affording adequate hyperthermia for killing cancer cells.^[41–43]

2.7. In Vivo PDT and PTT Combination Therapy

To evaluate actual therapeutic effect of FA-CNPs in vivo, SK-OV-3 tumor-bearing mice were stochastically divided into five groups for separate treatments as follows: 1) PBS, 2) PBS+laser, 3) FA-CNPs, 4) FA-CNPs+laser, and 5) FA-CNPs+Vc+laser. After 24 h postinjection, the tumor sites of the mice were exposed to 808 nm laser at 1.0 W cm^{-2} for 5 min. The tumor sizes were carefully monitored during 18 days after irradiation to qualitatively assess therapeutic effect of each group (Figure 5C). Similar to control groups, the tumor volumes of mice injected with FA-CNPs but without laser irradiation grew steadily, indicating low anti-cancer efficacy of FA-CNPs in this case. For the treatment group of FA-CNPs+laser, tumor growth was gradually and greatly suppressed during 18 days, although tumor size could not be immediately diminished in the early stage (5–6 days). $^1\text{O}_2$ -scavenger Vc was intratumorally injected into the tumors at 30 min before irradiation for evaluating the contribution of PDT to overall efficacy. As displayed in Figure 5C, this treatment was also effective in suppressing tumor growth, but exhibited only slightly less therapeutic effect than FA-CNPs+laser group. This should be probably attributed to relatively low $^1\text{O}_2$ yield of FA-CNPs under irradiation. Besides, no significant body weight loss or difference was found for all the tested groups (Figure 5D), suggesting the lesser side effects of FA-CNPs in vivo, if any. Remarkable cell apoptosis and necrosis was clearly seen in these tumors treated with both FA-CNPs and laser, demonstrating the potent ability of FA-CNPs to damage tumor cells under irradiation via synergistic hyperthermia and $^1\text{O}_2$ (Figure 5E).

Further, biosafety and side effects of the FA-CNPs in vivo were checked. The major organs of mice including heart, liver, spleen, lung, and kidney were harvested and analyzed by hematoxylin and eosin (H&E) staining after therapy. As shown in Figure 6, no distinct lesion and side effect were observed in these tested organs, indicating little harm of FA-CNPs to normal tissues. It revealed the safety of current treatments for living organisms.

3. Conclusions

In summary, a new NIR-absorbing A–D–A type small molecule-based sensitizing agent was developed for PDT and PTT combination therapy based on a simple yet general strategy. The encapsulation of CPDT into a folate functionalized polymer FA-PEG-PBLA yields FA-CNPs nanoparticles with good

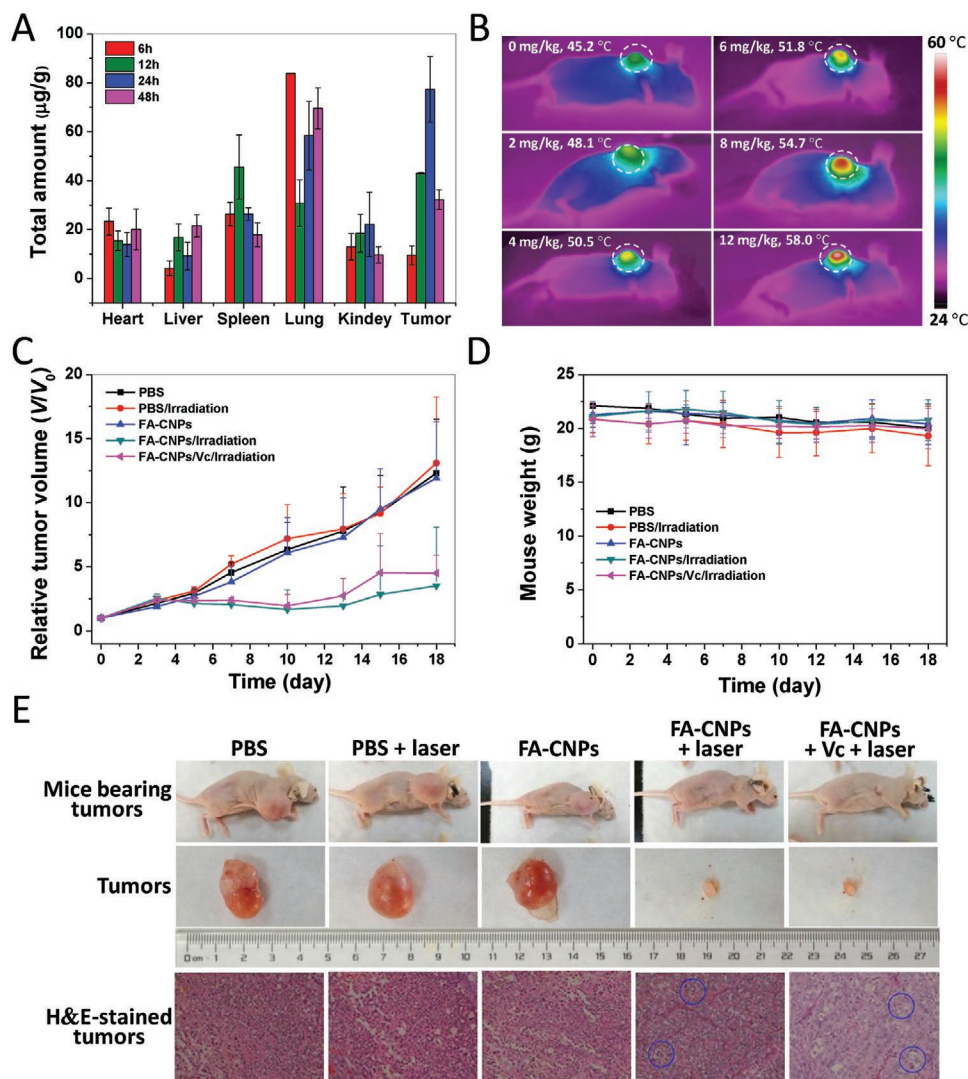


Figure 5. A) Ex vivo biodistribution of CPDT in various tissues of the mice treated with FA-CNPs at the dose of 4.0 mg kg⁻¹ at 6, 12, 24, and 48 h postinjection, respectively. B) IR thermal images of the SK-OV-3 tumor-bearing mice treated with FA-CNPs at various doses under 808 nm irradiation at 1.0 W cm⁻² for 5 min. C) Tumor growth profile of SK-OV-3 tumor-bearing mice after treatment with PBS, PBS+laser, FA-CNPs, FA-CNPs+laser, and FA-CNPs+Vc+laser, respectively. Irradiation conditions: 808 nm laser, 1.0 W cm⁻², 5 min. D) Body weight changes of mice in different treatment groups. E) Tumor images and H&E stained images of different groups of SK-OV-3 tumor-bearing mice after 18-day treatment, Scale bars: 20 μm. Cell apoptosis and necrosis are marked by blue circles.

biocompatibility, strong resistance to photobleaching, high PCE, and efficient ¹O₂ generation. FA-CNPs displayed strong absorption in NIR light region (750–870 nm), which would be good for light source selection and deep tissue penetration in phototherapy. Thanks to folate conjugation, cellular uptake, phototoxicity, and accumulation in tumor sites were obviously enhanced. In vivo test, FA-CNPs exhibited excellent tumor suppression under irradiation due to the possible PDT and PTT combination therapy. These results suggest that the A–D–A structured small molecule has great potential to develop single component sensitizing agents for NIR-triggered dual phototherapy of tumor, since their chemical structures can be facilely tuned to change HOMO and LUMO energy levels, further regulating photo energy dissipation pathway to meet the requirements of biomedicine applications.

4. Experimental Section

Materials: 6-bromo-4,4-dioctyl-4*H*-cyclopenta[1,2-*b*:5,4-*b'*]dithiophene-2-carbaldehyde and 2-(3-oxo-2,3-dihydro-1*H*-inden-1-ylidene)malononitrile were provided by Saipu Chemical products Co. (Henan, China). FA, β-benzyl-L-aspartate (BLA), PEG-bis(amine) (*M*_n = 3.350 kDa), PBS (0.01 M, pH 7.4), and 3-(4,5-dimethyl-2-thiazolyl)-2,5-diphenyl-2-*H*-tetrazolium bromide (MTT) were bought from Sigma Chemical Co. (St. Louis, MO, USA). Methoxypoly (ethylene glycol) amine (Me-PEG-NH₂) (*M*_n = 5.0 kDa), ethylene glycol, TEMP, ICG, and L-ascorbic acid (Vc) were obtained from Alfa Aesar (Shanghai, China). Triphosgene was provided by Aldrich Chemical Co. (Milwaukee, WI, USA). *N,N'*-dicyclohexylcarbodiimide and *N*-hydroxysuccinimide were purchased from Fluka (Buchs, Switzerland). DMEM, fetal bovine serum (FBS), penicillin, and streptomycin were provided by GibcoBRL (Invitrogen Corp., CA, USA). All other chemicals were obtained from local suppliers and used as received.

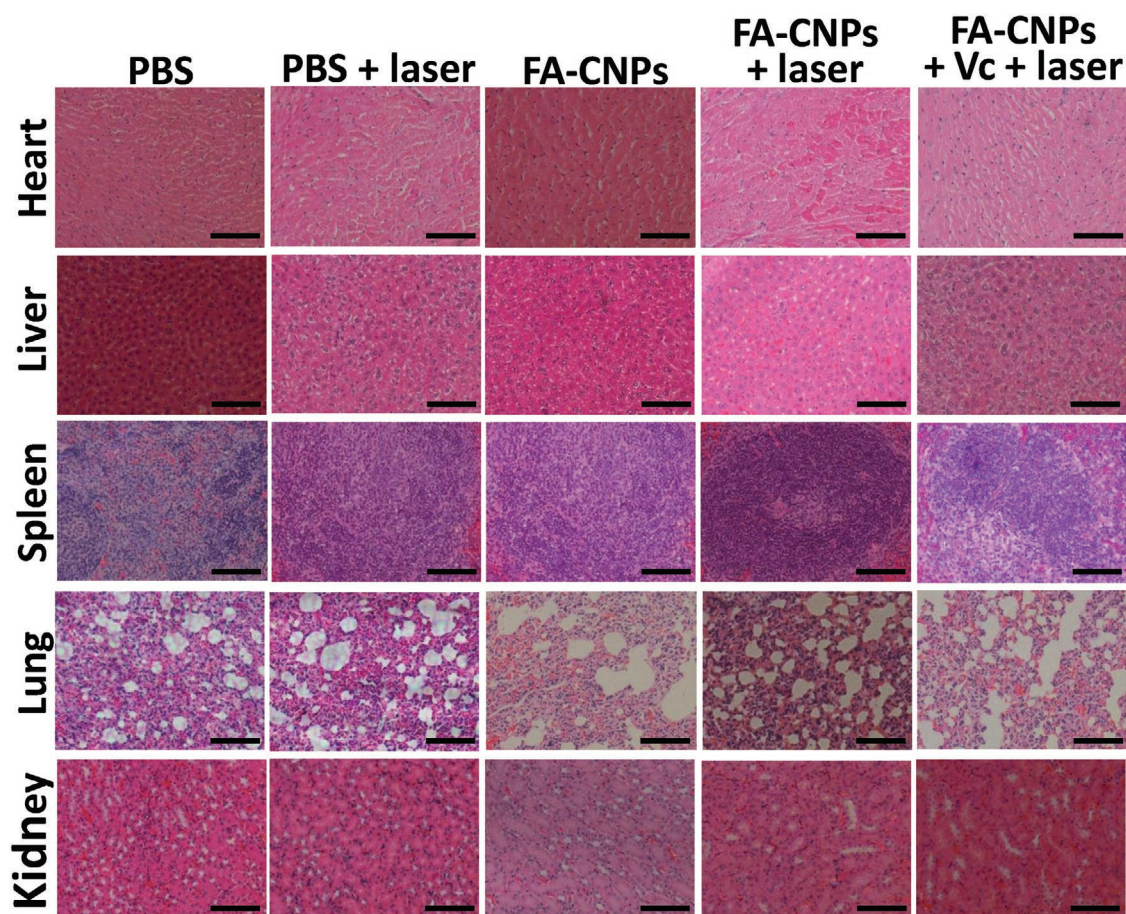


Figure 6. H&E-stained major organs after 18-day treatment. Scale bars: 20 μm .

Instruments: ^1H NMR and ^{13}C NMR spectra were recorded on a Bruker AVANCE III HD spectrometer (400 MHz, Fällanden, Switzerland) using CDCl_3 and $\text{DMSO}-d_6$ as the solvent and TMS as internal standard, respectively. The matrix-assisted laser desorption/ionization (MALDI-TOF) mass spectra were measured on a Bruker AutoflexIII LRF200-CID instrument (Bruker, Rheinstetten, Germany). UV-vis spectra were obtained on a Shimadzu UV-2550 (Shimadzu, Tokyo, Japan). Fluorescence spectra were collected on a Hitachi F-4600 (Hitachi, Tokyo, Japan) fluorescence spectrophotometer equipped with a xenon lamp excitation source. DLS were carried out on a Zetasizer Nano ZS90 (Malvern Instruments Co., UK). TEM was obtained using FEI Tecnai G2 Spirit TWIN at 120 kV (Hillsboro, FL, USA). IR thermal images were collected using IR thermal camera (TiS65, Fluke, Everett, WA, USA). EPR spectra were carried out on a Bruker EMXplus-6/1 spectrometer (Rheinstetten, Germany). H&E stained images were viewed by Nikon Eclipse Ti-U microscope (Tokyo, Japan). The NIR laser (808 nm) was purchased from Beijing Laserwave Optoelectronics Technology Co., Ltd. (LWIRL808-20W-F, Laserwave, Beijing, China).

Synthesis of CPDT: CPDT was synthesized according to the route shown in Scheme S1 of the Supporting Information. 6-bromo-4,4-bis-(2-ethyl-hexyl)-4H-cyclopenta[2,1-b:3,4-b']dithiophene-2-carbaldehyde (1, 0.2 g, 0.39 mmol), bis(pinacolato)diboron (0.12 g, 0.47 mmol), KOAc (1.154 g, 11.76 mmol), and DMSO (4 mL) were added into a two-necked round bottom flask. After purging with nitrogen for 0.5 h, $\text{Pd}(\text{dppf})\text{Cl}_2$ (9.6 mg, 0.012 mmol) was subsequently added into the above mixed solution under N_2 . The resulting mixture was heated to 80 $^\circ\text{C}$ and stirred for 8 h. The reaction mixture was then cooled down to room temperature, followed by being poured into 100 mL of deionized water. The mixture was extracted with chloroform three

times. The CHCl_3 layer was washed with brine and dried with anhydrous Na_2SO_4 . After concentration, the crude product was purified by column chromatography (silica gel, petroleum ether/dichloromethane = 6:1, v/v) to afford 2 as a dark-red solid (0.17 g, 85% yield). 2 (0.3 g, 0.349 mmol) and 2-(3-oxo-2,3-dihydro-1H-inden-1-ylidene)-malononitrile (3) (0.407 g, 2.1 mmol) were dissolved in 45 mL of dry CHCl_3 . 2.4 mL of pyridine was then added the solution under stirring. The mixed solution was refluxed for 15 h under nitrogen. The reaction mixture was cooled down to room temperature. The solution was concentrated and subsequently precipitated in excess CH_3OH . The crude product was collected by filtration and further purified by column chromatography (silica gel, petroleum ether/dichloromethane = 1:2, v/v) to yield CPDT as a deep-blue solid (0.28 g, 66.7% yield). ^1H NMR (400 MHz, CDCl_3): δ 8.86 (s, 2H), 8.62 (d, $J = 7.2$ Hz, 2H), 7.85 (d, $J = 6.5$ Hz, 2H), 7.81–7.46 (m, 6H), 7.17 (d, $J = 15.7$ Hz, 10H), 1.92 (s, 9H), 1.38 (dd, $J = 44.9, 40.5$ Hz, 9H), 1.22 (d, $J = 31.7$ Hz, 23H), 1.17–1.09 (m, 7H), 0.95 (t, $J = 31.1$ Hz, 35H), 0.81 (s, 4H), 0.75 (tt, $J = 22.0, 13.9$ Hz, 61H), 0.75 (tt, $J = 22.0, 13.9$ Hz, 69H), 0.68 (d, $J = 3.2$ Hz, 14H), 0.58 (t, $J = 7.0$ Hz, 11H). ^{13}C NMR (101 MHz, CDCl_3): δ 188.65 (s), 165.80 (s), 160.57 (s), 156.62 (s), 144.31 (s), 139.99 (s), 139.38 (s), 138.01 (d, $J = 8.7$ Hz), 137.68 (s), 136.85 (s), 134.88 (s), 134.17 (s), 125.16 (s), 123.49 (s), 120.62 (s), 119.48 (s), 115.04 (s), 77.28 (d, $J = 11.5$ Hz), 77.02 (s), 76.70 (s), 67.81 (s), 54.16 (s), 43.18 (s), 35.47 (d, $J = 5.2$ Hz), 34.06 (d, $J = 24.0$ Hz), 29.70 (s), 28.47 (s), 27.58 (s), 27.41 (d, $J = 30.0$ Hz), 22.78 (s), 14.07 (d, $J = 2.7$ Hz), 10.60 (d, $J = 6.1$ Hz). MS (MALDI-TOF): M^+ 1211.

Synthesis of FA-PEG-PBLA and Me-PEG-PBLA: The amphiphilic block copolymer FA-PEG-PBLA was prepared by ring-opening polymerization as reported in the previous work (Scheme S2, Supporting Information).^[53] Its structure was determined using ^1H NMR spectra (400 MHz, DMSO)

δ 8.23 (d, $J = 28.5$ Hz, 1H), 8.16–7.82 (m, 1H), 7.40–7.20 (m, 12H), 6.80 (d, $J = 117.0$ Hz, 1H), 6.03–4.95 (m, 5H), 6.03–4.64 (m, 6H), 6.03–4.85 (m, 5H), 6.03–4.43 (m, 8H), 6.03–4.39 (m, 8H), 6.03–4.31 (m, 8H), 6.03–4.25 (m, 8H), 6.03–4.19 (m, 8H), 6.03–3.89 (m, 10H), 6.03–3.56 (m, 12H), 6.03–3.43 (m, 85H), 3.43–3.17 (m, 3H), 2.89 (dd, $J = 47.1, 29.6$ Hz, 3H), 3.03–2.59 (m, 5H), 2.50 (s, 5H). The control copolymer Me-PEG-PBLA was synthesized according to the similar procedure to that of FA-PEG-PBLA (Scheme S2, Supporting Information). The degree of polymerization of PBLA segment in FA-PEG-PBLA was estimated by the integral area ratio of the proton peak (a) at 7.30 ppm corresponding to benzene ring to the proton peak (b) at 3.51 ppm assigning to methylene in ethylene glycol unit (Figure S4, Supporting Information).

Preparation of FA-CNPs Nanoparticles: FA-CNPs nanoparticles were prepared by nanoprecipitation method, followed by subsequent dialysis. In detail, 5 mg of CPDT was dissolved in 1 mL of CHCl_3 . The as-prepared CPDT solution was dropwise added into to 50 mL of FA-PEG-PBLA in DMSO (0.5 mg mL^{-1}). The CHCl_3 was removed from the mixed solution under a stream of nitrogen gas. After complete removal of CHCl_3 , the mixture was transfer to dialysis tubs (cut-off 3.5 K Mw) to dialyze two days, followed by freeze drying. 28.5 mg of FA-CNPs nanoparticles was obtained as a blue powder (95% yield). The FA unconjugated nanoparticles (named as Me-CNPs) were prepared as the control sample by the same process except replacing FA-PEG-PBLA with Me-PEG-PBLA.

Fluorescence Quantum Yield: Fluorescent quantum yields (Φ) of CPDT and FA-CNPs were determined using rhodamine B as reference ($\Phi = 0.73$ in ethanol), whose maximal emission was around 540 nm under 500 nm excitation. Rhodamine B in ethanol, CPDT in CHCl_3 , and FA-CNPs in PBS buffer with the similar maximum absorbance (<0.05) were excited under 540, 746, and 750 nm, respectively, and the corresponding fluorescence spectra were collected. The fluorescence quantum yields (Φ) were estimated by integration analysis of emission intensity of their corresponding fluorescent spectra according to the following equation

$$\Phi_1 = \Phi_B \times (\text{Abs}_B \times F_1 \times \lambda_{\text{exB}} \times \eta_1) / (\text{Abs}_1 \times F_B \times \lambda_{\text{ex1}} \times \eta_B) \quad (1)$$

where Φ is the fluorescent quantum yield, the subscripts 1 and B represent the objects to be measured and the reference standard (rhodamine B), respectively. Abs is absorption value at the excitation wavelength, F is fluorescence integral area, and η is refractive index of the solvent.

PTT Effect and PCE: Temperature changes of FA-CNPs in PBS with various concentrations (0, 30, 90, 120, 180, and $250 \mu\text{g mL}^{-1}$) under 808 nm laser irradiation at 0.7 W cm^{-2} were monitored using an IR image camera (TiS65, Fluke). Besides, $180 \mu\text{g mL}^{-1}$ of FA-CNPs in PBS under 808 nm laser irradiation at various power densities (0.3, 0.5, 0.8, 1.2, 1.5, and 2.0 W cm^{-2}) were also carefully studied. PCE of was measured according to the following process. FA-CNPs in PBS ($180 \mu\text{g mL}^{-1}$) were exposed to 808 nm irradiation at 0.7 W cm^{-2} for 5 min. Subsequently, the laser was removed and the solution was cooled down to room temperature. During this process, the solution temperatures were continuously recorded by an IR image camera (TiS65, Fluke). PCE was then calculated based on the reported method in the literature.^[54]

Singlet Oxygen Detection and Singlet Oxygen Quantum Yield: DPBF was utilized as a probe to detect $^1\text{O}_2$ generation. In this experiment, 1 mL of FA-CNPs in PBS with different concentrations such as 0, 30, 60, 120, and $180 \mu\text{g mL}^{-1}$ was separately mixed with 2.23 mL of DPBF in DMSO ($0.1 \times 10^{-3} \text{ M}$) in a dark under continuous stirring. UV-vis spectra of the mixed solutions were measured at an interval of 1 min under 808 nm laser irradiation at 0.7 W cm^{-2} . The absorption intensity of DPBF at 417 nm was collected and plotted as a curve of absorption intensities over time. To measure singlet oxygen quantum yield (Φ) of FA-CNPs, DPBF and ICG were used as probe and reference ($\Phi_{\text{ICG}} = 0.14$),^[44] respectively. Two mixed PBS solutions ($180 \mu\text{g mL}^{-1}$ of FA-CNPs + $0.1 \times 10^{-3} \text{ M}$ of DPBF as well as $30 \mu\text{g mL}^{-1}$ of ICG + $0.1 \times 10^{-3} \text{ M}$ of DPBF) were irradiated by 808 nm laser at 0.7 W cm^{-2} . During irradiation, the absorbance of DPBF at 417 nm was recorded at an interval of 30 s. Φ of FA-CNP was calculated based on the following formula

$$\Phi_1 = \Phi_{\text{ICG}} \times (S_1/S_{\text{ICG}}) \times (F_{\text{ICG}}/F_1) \quad (2)$$

where the subscripts 1 and ICG represent FA-CNPs and ICG, respectively. S_1 and S_{ICG} are the photobleaching rates of DPBF in the presence of FA-CNPs and ICG, respectively. F is absorption correction factor, which can be calculated from $F = 1 - 10^{-\text{OD}}$ (OD is the absorbance of the FA-CNPs and ICG at 808 nm).

ESR: ESR technique can be applied to affirm the type of ROS. In this test, TEMP was selected as the spin-trapping agent of $^1\text{O}_2$. 1 mL of FA-CNPs in D_2O ($200 \mu\text{g mL}^{-1}$) was mixed with 10 μL of TEMP. The mixture was then transferred into the capillary tube. The mixture was then irradiated using 808 nm laser at 1.0 W cm^{-2} for 0, 2, 5, and 10 min, respectively. After irradiation, ESR measurement was immediately performed on a Bruker EMXplus-6/1 spectrometer.

Cellular Culture and Cell Uptake: 5×10^4 cells per well of HeLa cells were seeded onto 12-well plates and cultured in DMEM supplemented with FBS (10%) and penicillin-streptomycin (1%) at 37°C in a humid air atmosphere containing 5% CO_2 . After 24 h, the culture media was replaced with 1.5 mL of fresh one containing FA-CNPs ($180 \mu\text{g mL}^{-1}$, $30 \mu\text{g mL}^{-1}$ based on CPDT) and the free CPDT ($30 \mu\text{g mL}^{-1}$) (0.5% THF, V/V), respectively. After incubation for 6, 24, and 48 h, the cells were washed with PBS and handled with 0.05% of trypsin-EDTA, followed by cell counting and ultrasonication. The CPDT was extracted from HeLa cells using chloroform. The uptake amount of CPDT by HeLa cells was determined by UV-vis analysis based on the standard curve.

Dark Toxicity and Phototoxicity of FA-CNPs: The dark toxicity of FA-CNPs was evaluated as following: After cell attachment, the culture media was replaced with 100 μL of fresh one containing different concentrations of FA-CNPs such as 0, 30, 60, 90, 120, 180, and $250 \mu\text{g mL}^{-1}$, followed by incubation for another 24 h. The cell viability was assessed by widely used MTT assay. All data are based on four parallel experiments. The phototoxicity of FA-CNPs was evaluated according to the similar procedure, but the culture media was replaced with 100 μL of fresh one containing FA-CNPs, FA-CNPs+Vc ($0.1 \times 10^{-3} \text{ M}$ of Vc), FA-PEG-PBLA, and FA-PEG-PBLA+Vc ($0.1 \times 10^{-3} \text{ M}$ of Vc) with different concentrations of FA-CNPs and FA-PEG-PBLA from 0 to $250 \mu\text{g mL}^{-1}$ ($[\text{FA-CNPs}] = [\text{FA-PEG-PBLA}]$), followed by incubation for another 4 h. Subsequently, the cells were washed with PBS and replaced with fresh culture media. The samples were exposed to 808 nm laser irradiation at 0.7 W cm^{-2} for 5 min. Irradiated cells were then incubated at 37°C for another 24 h and cell viability was also evaluated using MTT assay. All data are based on four parallel experiments.

Intracellular $^1\text{O}_2$ Generation Study: After HeLa cell attachment, the original culture media was replaced with 2 mL of fresh one with and without FA-CNPs ($180 \mu\text{g mL}^{-1}$), followed by 5 h of incubation. 2 μL of DCFH-DA in DMSO ($1 \times 10^{-3} \text{ M}$) (water-insoluble DCFH-DA was dissolved in DMSO and then diluted by DMEM until the DMSO concentration is lower than 0.1%) was added into the cells for another 1 h of incubation and subsequently the treated cells were irradiated using 808 nm laser at 0.7 W cm^{-2} for 5 min. The fluorescence images of cells were then acquired using a confocal laser scanning microscopy (FV1000-IX81, Olympus) at 488 nm excitation.

Animal Tumor Model: All animal experiments were conducted in accordance with relevant laws and agency guidelines. The about six weeks old female BALB/c mice were provided by SPF (Beijing) Biotechnology Co., Ltd. (Beijing, China). The about 2 mm^3 SK-OV-3 tumor tissue mass was subcutaneously injected into the right auxiliary space of nude mice to establish a model of SK-OV-3 tumor-bearing mice. The mice with tumor volumes at about 100–120 mm^3 were subsequently used.

Tissue Biodistribution: FA-CNPs in PBS ($180 \mu\text{g mL}^{-1}$) were intravenously injected into the SK-OV-3 tumor-bearing mice ($\approx 20 \text{ g}$) at the dose of 4 mg kg^{-1} . Afterward, the tumor, heart, liver, spleen, lung, and kidney were removed and weighed at 6, 12, 24, and 48 h postinjection, respectively, followed by the extraction of CPDT from these tissues using CHCl_3 . The amount of CPDT in tested tissues was measured using UV-vis spectral analysis.

In Vivo Photothermal Effect: The mice bearing SK-OV-3 tumor were injected with FA-CNPs at various doses including 0, 2, 4, 6, 8, and

12 mg kg⁻¹ through the tail vein. After 24 h postinjection, IR camera was used to monitor the temperatures on the surface of tumor site under 808 nm laser irradiation at 1.0 W cm⁻².

Anticancer Efficacy: The mice bearing SK-OV-3 tumor were randomly divided into five groups ($n = 5$ per group). They were named as PBS, PBS+laser, FA-CNPs, FA-CNPs+laser, and FA-CNPs+Vc+laser, respectively. For each group, FA-CNPs in PBS were injected through the tail vein at the dose of 4.0 mg kg⁻¹. Vc was directly injected into the tumor site at the dose of 5 mg kg⁻¹ at 30 min before irradiation. At 24 h postinjection, the tumor sites were irradiated by 808 nm laser at 1.0 W cm⁻² for 5 min. After laser treatment, the mouse body weights and the tumor volumes were measured at different time within 18 days. The tumor volume was calculated according to the equation as follows

$$\text{Volume} = \text{Width}^2 \times \text{Length} / 2 \quad (3)$$

After 18 days, treated SK-OV-3 tumor-bearing mice were sacrificed. Tumors and main organs such as heart, liver, spleen, lung, and kidney were harvested for H&E staining. H&E stained images were viewed by microscope (Eclipse Ti-U, Nikon).

Supporting Information

Supporting Information is available from the Wiley Online Library or from the author.

Acknowledgements

This research was supported by the National Natural Science Foundation of China (Grant Nos. 51703163 and 21604063), the Natural Science Foundation of Tianjin (18JCZDJC34600 and 18JCYBJC86700), and the Program for Prominent Young College Teachers of Tianjin Educational Committee.

Conflict of Interest

The authors declare no conflict of interest.

Author Contributions

Z.H., L.Z., and Q.Z. contributed equally to this work. They performed syntheses, characterizations, photothermal and photodynamic properties studies and combination phototherapy of mice. M.C. and C.L. helped with the synthesis of the materials. H.Z. provided assistance in animal experiments. Y.L. and Y.C. designed this project and cowrote the paper.

Keywords

A–D–A structures, dual phototherapy, photothermal agents, singlet oxygen, structure design

Received: December 11, 2019

Revised: January 31, 2020

Published online:

- [1] J. Li, K. Pu, *Chem. Soc. Rev.* **2019**, *48*, 38.
 [2] Y. Liu, P. Bhattarai, Z. Dai, X. Chen, *Chem. Soc. Rev.* **2019**, *48*, 2053.
 [3] S. B. Brown, E. A. Brown, I. Walker, *Lancet Oncol.* **2004**, *5*, 497.

- [4] C. Yin, G. Wen, C. Liu, B. Yang, S. Lin, J. Huang, P. Zhao, S. H. D. Wong, K. Zhang, X. Chen, G. Li, X. Jiang, J. Huang, K. Pu, L. Wang, L. Bian, *ACS Nano* **2018**, *12*, 12201.
 [5] D.-W. Zheng, B. Li, C.-X. Li, J.-X. Fan, Q. Lei, C. Li, Z. Xu, X.-Z. Zhang, *ACS Nano* **2016**, *10*, 8715.
 [6] L. Yang, H. Li, D. Liu, H. Su, K. Wang, G. Liu, X. Luo, F. Wu, *Colloids Surf., B* **2019**, *182*, 110345.
 [7] J. Choi, S.-E. Lee, J.-S. Park, S. Y. Kim, *Biotechnol. Bioeng.* **2018**, *115*, 1340.
 [8] B. Jang, J.-Y. Park, C.-H. Tung, I.-H. Kim, Y. Choi, *ACS Nano* **2011**, *5*, 1086.
 [9] J. Peng, L. Zhao, X. Zhu, Y. Sun, W. Feng, Y. Gao, L. Wang, F. Li, *Biomaterials* **2013**, *34*, 7905.
 [10] H. S. Jung, P. Verwilt, A. Sharma, J. Shin, J. L. Sessler, J. S. Kim, *Chem. Soc. Rev.* **2018**, *47*, 2280.
 [11] Y. Cai, W. Si, W. Huang, P. Chen, J. Shao, X. Dong, *Small* **2018**, *14*, 1704247.
 [12] Y. Chen, L. Li, W. Chen, H. Chen, J. Yin, *Chin. Chem. Lett.* **2019**, *30*, 1353.
 [13] H. S. Jung, J.-H. Lee, K. Kim, S. Koo, P. Verwilt, J. L. Sessler, C. Kang, J. S. Kim, *J. Am. Chem. Soc.* **2017**, *139*, 9972.
 [14] S. Luo, X. Tan, S. Fang, Y. Wang, T. Liu, X. Wang, Y. Yuan, H. Sun, Q. Qi, C. Shi, *Adv. Funct. Mater.* **2016**, *26*, 2826.
 [15] X. Tan, S. Luo, L. Long, Y. Wang, D. Wang, S. Fang, Q. Ouyang, Y. Su, T. Cheng, C. Shi, *Adv. Mater.* **2017**, *29*, 1704196.
 [16] Y. Huang, N. He, Y. Wang, D. Shen, Q. Kang, R. Zhao, L. Chen, *J. Mater. Chem. B* **2019**, *7*, 1149.
 [17] M. Asadian-Birjand, J. Bergueiro, S. Wedepohl, M. Calderón, *Macromol. Biosci.* **2016**, *16*, 1432.
 [18] Y. Cai, P. Liang, Q. Tang, X. Yang, W. Si, W. Huang, Q. Zhang, X. Dong, *ACS Nano* **2017**, *11*, 1054.
 [19] Y. Cai, P. Liang, Q. Tang, W. Si, P. Chen, Q. Zhang, X. Dong, *ACS Appl. Mater. Interfaces* **2017**, *9*, 30398.
 [20] Q. Wang, Y. Dai, J. Xu, J. Cai, X. Niu, L. Zhang, R. Chen, Q. Shen, W. Huang, Q. Fan, *Adv. Funct. Mater.* **2019**, *29*, 1901480.
 [21] Z. Guo, Y. Zou, H. He, J. Rao, S. Ji, X. Cui, H. Ke, Y. Deng, H. Yang, C. Chen, Y. Zhao, H. Chen, *Adv. Mater.* **2016**, *28*, 10155.
 [22] Q. Tang, W. Si, C. Huang, K. Ding, W. Huang, P. Chen, Q. Zhang, X. Dong, *J. Mater. Chem. B* **2017**, *5*, 1566.
 [23] J. Chen, X. Tan, S. Luo, L. Long, L. Liu, Z. Liu, Y. Wang, C. Shi, *J. Innovative Opt. Health Sci.* **2018**, *11*, 1850016.
 [24] Y. Ma, M. Zhang, P. Li, Z. Han, L. Wu, T. Li, Z. Wang, W. Gao, T. Deng, Y. Gu, *Part. Part. Syst. Character.* **2017**, *34*, 1700076.
 [25] Y. Jiao, K. Liu, G. Wang, Y. Wang, X. Zhang, *Chem. Sci.* **2015**, *6*, 3975.
 [26] J. Tian, J. Zhou, Z. Shen, L. Ding, J.-S. Yu, H. Ju, *Chem. Sci.* **2015**, *6*, 5969.
 [27] C. S. Foote, *Photochem. Photobiol.* **1991**, *54*, 659.
 [28] Y.-L. Chen, S.-W. Li, Y. Chi, Y.-M. Cheng, S.-C. Pu, Y.-S. Yeh, P.-T. Chou, *ChemPhysChem* **2005**, *6*, 2012.
 [29] S. Xu, Y. Yuan, X. Cai, C.-J. Zhang, F. Hu, J. Liang, G. Zhang, D. Zhang, B. Liu, *Chem. Sci.* **2015**, *6*, 5824.
 [30] J. Li, D. Cui, J. Huang, S. He, Z. Yang, Y. Zhang, Y. Luo, K. Pu, *Angew. Chem., Int. Ed.* **2019**, *58*, 12680.
 [31] Y. Jiang, J. Li, Z. Zeng, C. Xie, Y. Lyu, K. Pu, *Angew. Chem., Int. Ed.* **2019**, *58*, 8161.
 [32] J. Li, D. Cui, Y. Jiang, J. Huang, P. Cheng, K. Pu, *Adv. Mater.* **2019**, *31*, 1905091.
 [33] N. Qiu, H. Zhang, X. Wan, C. Li, X. Ke, H. Feng, B. Kan, H. Zhang, Q. Zhang, Y. Lu, Y. Chen, *Adv. Mater.* **2017**, *29*, 1604964.
 [34] Y.-Q.-Q. Yi, H. Feng, M. Chang, H. Zhang, X. Wan, C. Li, Y. Chen, *J. Mater. Chem. A* **2017**, *5*, 17204.
 [35] M. Chang, Y. Wang, Y.-Q.-Q. Yi, X. Ke, X. Wan, C. Li, Y. Chen, *J. Mater. Chem. A* **2018**, *6*, 8586.
 [36] B. Kan, H. Feng, X. Wan, F. Liu, X. Ke, Y. Wang, Y. Wang, H. Zhang, C. Li, J. Hou, Y. Chen, *J. Am. Chem. Soc.* **2017**, *139*, 4929.

- [37] Y. Cai, Z. Wei, C. Song, C. Tang, X. Huang, Q. Hu, X. Dong, W. Han, *Chem. Commun.* **2019**, 55, 8967.
- [38] H. Elnakat, M. Ratnam, *Adv. Drug Delivery Rev.* **2004**, 56, 1067.
- [39] M. Geszke, M. Murias, L. Balan, G. Medjahdi, J. Korczynski, M. Moritz, J. Lulek, R. Schneider, *Acta Biomater.* **2011**, 7, 1327.
- [40] J. D. Byrne, T. Betancourt, L. Brannon-Peppas, *Adv. Drug Delivery Rev.* **2008**, 60, 1615.
- [41] Y. Lyu, Y. Fang, Q. Miao, X. Zhen, D. Ding, K. Pu, *ACS Nano* **2016**, 10, 4472.
- [42] J. Qi, Y. Fang, R. T. K. Kwok, X. Zhang, X. Hu, J. W. Y. Lam, D. Ding, B. Z. Tang, *ACS Nano* **2017**, 11, 7177.
- [43] C. Liang, S. Diao, C. Wang, H. Gong, T. Liu, G. Hong, X. Shi, H. Dai, Z. Liu, *Adv. Mater.* **2014**, 26, 5646.
- [44] Y. Liu, K. Ai, J. Liu, M. Deng, Y. He, L. Lu, *Adv. Mater.* **2013**, 25, 1353.
- [45] Y. Deng, L. Huang, H. Yang, H. Ke, H. He, Z. Guo, T. Yang, A. Zhu, H. Wu, H. Chen, *Small* **2017**, 13, 1602747.
- [46] Z. B. Sun, H. H. Xie, S. Y. Tang, X. F. Yu, Z. N. Guo, J. D. Shao, H. Zhang, H. Huang, H. Y. Wang, P. K. Chu, *Angew. Chem., Int. Ed.* **2015**, 54, 11526.
- [47] T. Yang, L. Liu, Y. Deng, Z. Guo, G. Zhang, Z. Ge, H. Ke, H. Chen, *Adv. Mater.* **2017**, 29, 1700487.
- [48] M. Guo, H. Mao, Y. Li, A. Zhu, H. He, H. Yang, Y. Wang, X. Tian, C. Ge, Q. Peng, X. Wang, X. Yang, X. Chen, G. Liu, H. Chen, *Biomaterials* **2014**, 35, 4656.
- [49] K. Nawalany, A. Rusin, M. Kępczyński, A. Mikhailov, G. Kramer-Marek, M. Śnietura, J. Połtowicz, Z. Krawczyk, M. Nowakowska, *J. Photochem. Photobiol., B* **2009**, 97, 8.
- [50] S. M. Moghimi, A. C. Hunter, J. C. Murray, *Pharmacol. Rev.* **2001**, 53, 283.
- [51] L. Zhang, M. Yang, Q. Wang, Y. Li, R. Guo, X. Jiang, C. Yang, B. Liu, *J. Controlled Release* **2007**, 119, 153.
- [52] A. Tahmasbi Rad, C.-W. Chen, W. Aresh, Y. Xia, P.-S. Lai, M.-P. Nieh, *ACS Appl. Mater. Interfaces* **2019**, 11, 10505.
- [53] L. Zhao, T.-H. Kim, K. M. Huh, H.-W. Kim, S. Y. Kim, *J. Biomater. Appl.* **2013**, 28, 434.
- [54] W. Ren, Y. Yan, L. Zeng, Z. Shi, A. Gong, P. Schaaf, D. Wang, J. Zhao, B. Zou, H. Yu, G. Chen, E. M. B. Brown, A. Wu, *Adv. Healthcare Mater.* **2015**, 4, 1526.